



# Comparisons Between Two Different Three-Dimensional Arc Plasma Torch Simulations

B. Selvan and K. Ramachandran

(Submitted January 29, 2009; in revised form April 1, 2009)

Several numerical models have been developed to study the characteristics of an arc inside the non-transferred plasma torch. A few of them have considered complete geometry of cathode and anode nozzle (type I) whereas others have considered only anode nozzle with cathode tip (type II). In this work, a three-dimensional model is developed to simulate Ar-N<sub>2</sub> arc in type I and type II geometries. Various combinations of the arc length and arc core radius are predicted for the torch power that corresponds to given gas flow rate and current. Various combinations of the same and minimum entropy production for all cases could not be predicted in type II geometry. The difference between velocities predicted in both geometries is larger than that between temperatures. Three-dimensional effect in the plasma jet thermo-fluid fields demises along the axial direction. Torch efficiencies and arc voltages predicted in both geometries are comparable with measurements.

**Keywords** influence of process parameters, minimum entropy production, modeling, plasma arc modeling, plasma jet modeling

## 1. Introduction

Reproducibility of the coating quality is one of the serious problems to be resolved in the plasma spray process. Random fluctuation of an arc inside the plasma torch is one of the main factors that affect the coating quality strongly. Also, the same affects life of electrodes and electro-thermal efficiency of the torch. Arc movement inside the torch is the result of imbalance between gas dynamic force due to incoming fluid flow and electromagnetic force due to current flow. Various plasma torch designs have been developed to limit the arc fluctuations, improve the electro-thermal efficiency, and enhance the life of the electrodes. Absolute knowledge on the arc behavior inside the torch and effect of operating parameters on it may help to design torches with higher electro-thermal efficiency and to control the arc.

An arc inside the torch has been characterized experimentally (Ref 1-7) and numerically (Ref 8-21). Unfortunately, experiments have been limited by involvement of high cost equipments and lack of understanding of the results obtained. Numerical modeling is the best tool to study the arc behavior and heat transfer process inside the

plasma spray torch. Both two-dimensional (Ref 8-11, 19, 21) and three-dimensional (Ref 12-18) models have been developed to understand the arc behavior inside the plasma torch. Two-dimensional models (Ref 8, 10, 21) have assumed the anode arc attachment in the form of a ring, which is unrealistic boundary condition to simulate the arc inside the torch. The arc-root position in a DC plasma torch has been determined using two-dimensional model (Ref 9). Gonzalez et al. (Ref 11) have predicted nonsymmetric temperature and velocity profiles at the nozzle exit with lateral arc attachment in two-dimensional model. Two-dimensional numerical model with non-LTE has been developed to study the arc-anode attachment in DC electric arcs (Ref 19).

Anode-arc attachment has been assumed as a constricted spot on the anode in three-dimensional models (Ref 12-18, 20). Li et al. (Ref 12) and Li and Pfender (Ref 20) have developed a steady model for Ar plasma and determined the arc attachment position using Steenbeck's minimum principle. Trelles and Heberlein (Ref 15) have simulated the arc behavior in different plasma torches. This model describes the dynamics of the arc without any further assumptions on the reattachment process except for the use of an artificially high electrical conductivity near the electrodes. This high electrical conductivity technique allows the free movement of the arc attachment along the anode surface and the formation of a new arc attachment if some part of the arc gets close enough to the anode surface. Trelles et al. (Ref 18) have presented three-dimensional arc reattachment model capable of mimicking the physical reattachment process. In their model, the arc breakdown is assumed to occur, at a particular location, when the maximum of the magnitude of the local electric field in the direction normal to the anode exceeds the

B. Selvan and K. Ramachandran, School of Mechanical and Building Sciences, VIT University, Vellore, India. Contact e-mail: ramspg@yahoo.com.

pre-specified breakdown electric field. To establish the new arc attachment, a cylindrical breakdown channel, in which the value of the electrical conductivity is maximum of either equilibrium electrical conductivity of the plasma or an electrical conductivity that characterize the breakdown process, is introduced between the anode surface and the arc in the direction normal to the anode. Some of these three-dimensional models (Ref 12, 15, 18, 20) have considered complete geometry of cathode and anode nozzle (type I). Although type I geometry includes the complete geometry of the plasma torch, the realistic boundary conditions can be achieved only by considering the solid wall of the anode and near electrode sheath in the model.

Baudry et al. (Ref 13) have developed an unsteady model for Ar-H<sub>2</sub> plasma and studied the arc behavior and voltage fluctuations in the re-strike mode. In this model, the breakdown of the arc occurs when the electric field is higher than a specific value. The creation of a new attachment spot by re-arcing is favored by the modification of the boundary condition for the electric potential at the anode wall. Moreau et al. (Ref 14) have developed a three-dimensional model to study the re-strike mode operation of a DC plasma spray torch. In this model, the electric field between the edge of the arc column and the anode wall is calculated in the whole boundary layer that covers the anode surface defined by an electrical conductivity lower than 150 Ω m<sup>-1</sup> and compared with a critical electric field over which breakdown process can occur. The new arc-root attachment is introduced by imposing a hot gas column that connects the arc column to the anode wall at the location where the electric field was found to be greater than the critical field. Using the similar model, the effect of operating parameters on the motion of the anode root attachment has been studied (Ref 16). Ramachandran et al. (Ref 17) have simulated the plasma arc inside the torch under stationary condition and have predicted size of the arc using an original/thermodynamic principle of minimum entropy production without including the radiation loss to calculate entropy production. These models have considered the geometry of anode nozzle and cathode tip (type II) only. Coudert and Rat (Ref 22) have studied the existence of a fluctuation due to the Helmholtz oscillations of the cold gas pressure in the cavity comprised between the gas injection ring and the cathode tip of the plasma torch.

In the present study, a steady state model is developed to simulate Ar-N<sub>2</sub> arc in type I and type II geometries of the DC nontransferred plasma torch. The effects of arc current and gas flow rate on characteristics of the arc and temperature and velocity distributions inside the torch predicted in type I and type II geometries are discussed. The nozzle exit velocity and temperature profiles obtained from type I and type II geometries are compared. To clarify the effect of nozzle exit velocity and temperature profiles predicted from type I and type II geometries on the plasma jet velocity and temperature, a plasma jet is simulated and its velocity and temperature distributions are compared.

## 2. Model Description

### 2.1 Plasma Arc

The following assumptions are used in the model to simulate the plasma arc.

1. Plasma flow is steady
2. The plasma is in local thermodynamic equilibrium (LTE)
3. The plasma optically thin
4. The flow inside the plasma torch is laminar and incompressible.

A set of governing equations to simulate the arc inside the DC nontransferred plasma torch can be expressed in the simplified form as

$$\text{div}(\rho \bar{V} \phi) - \text{div}(\Gamma_{\phi} \text{grad} \phi) = S_{\phi} \quad (\text{Eq 1})$$

Table 1 shows the dependent variable/property ( $\phi$ ), diffusion coefficient ( $\Gamma_{\phi}$ ), and source term ( $S_{\phi}$ ) for each equation. The first and second terms in the left hand side of the Eq 1, where  $\rho$  is mass density, represent the transport of  $\phi$  by means of convection and diffusion, respectively. In Table 1,  $u$ ,  $v$ ,  $w$ ,  $h$ ,  $j$ ,  $\mu_1$ ,  $Cp$ ,  $\lambda$ ,  $S_R$ ,  $\nabla P$ ,  $A_x$ ,  $A_y$  &  $A_z$ ,  $\mu_0$ ,  $B$ ,  $\phi$ , and  $\sigma$  are, respectively,  $x$ -velocity,  $y$ -velocity,  $z$ -velocity, enthalpy, current density, laminar or molecular viscosity, specific heat capacity at constant pressure, thermal conductivity, volumetric radiation loss, pressure gradient, vector potential in  $x$ ,  $y$  and  $z$  directions, magnetic permeability, magnetic field, electric potential, and electrical conductivity. The source terms in the momentum equations are pressure gradient and an electromagnetic force and the same in energy equation are the joule heating and the net radiation loss. Governing equations are solved by SIMPLE algorithm used in commercial CFD software FLUENT 6.3. The plasma gas is a mixture of argon and nitrogen. The radiation emission coefficients of argon and nitrogen are taken from (Ref 23, 24). The radiation loss ( $S_R$ ) of Ar-N<sub>2</sub> mixture is calculated using Eq 2.

$$S_R = \epsilon n_{Ar} x_{Ar} + \epsilon n_{N_2} x_{N_2}, \quad (\text{Eq 2})$$

where  $\epsilon n$  and  $x$  are net radiation emission coefficient and mole fraction, respectively. Thermodynamic and transport properties of the plasma gases are taken from Ref 25.

**Table 1** Dependent variable/property ( $\phi$ ), diffusion coefficient ( $\Gamma_{\phi}$ ), and source term ( $S_{\phi}$ ) in each equation used to simulate the plasma arc

Equation	$\phi$	$\Gamma_{\phi}$	$S_{\phi}$
Continuity	1	0	0
Momentum	$u$ , $v$ , & $w$	$\mu_1$	$-\nabla P + \vec{j} \times \vec{B}$
Energy	$h$	$\lambda/Cp$	$(j^2/\sigma) - S_R$
Electric potential	$\phi$	$\sigma$	0
Magnetic vector potential	$A_x$ , $A_y$ , & $A_z$	1	$-\mu_0 \vec{j} (\vec{B} = \nabla \times \vec{A})$

Type I and type II computational geometries of the plasma torch are shown in Fig. 1(a) and (b), respectively. The geometry of the torch (type I and type II) used in numerical simulations is same as that used in experiments. It is generated with 1,05,600 and 76,240 calculation points in type I and type II geometries, respectively. Mesh is refined near wall region, and construction of the same is similar in both geometries. The boundary conditions used in type I and type II geometries are shown in Table 2.

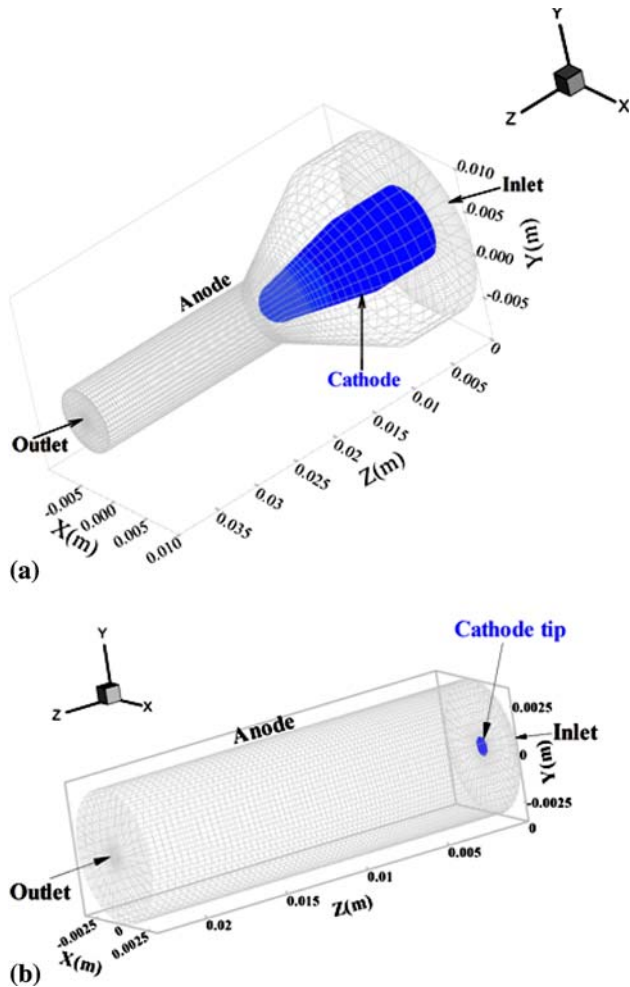


**Fig. 1** Computational geometry of the plasma torch (a) type I and (b) type II

The radial current density profile used at the cathode in type I geometry is given by

$$j(r) = j_{\max} \left[ 1 - \left( \frac{r}{R_{\text{arc}}} \right)^n \right], \quad (\text{Eq 3})$$

where  $r$  and  $n$  are radial distance from the torch axis and a parameter that specify the shape of the current density profile, respectively, and the maximum current density ( $j_{\max}$ ) at the axis is fixed with certain value to ensure the integration of  $j(r)$  over the cathode equals to the applied current. As an example, for a specified current of 400 A,  $j_{\max}$ ,  $n$ , and arc core radius ( $R_{\text{arc}}$ ) are  $6.46 \times 10^7 \text{ A m}^{-2}$ , 2.0, and  $1.8 \times 10^{-3} \text{ m}$ , respectively. The linear current density profile used at the cathode tip and inlet in Type II geometry is given by

$$j(r) = \frac{3I}{\pi R_{\text{arc}}^2} \left[ 1 - \frac{r}{R_{\text{arc}}} \right], \quad (\text{Eq 4})$$

where the maximum current density ( $j_{\max} = \frac{3I}{\pi R_{\text{arc}}^2}$ ) on the axis depends on the current ( $I$ ) and arc core radius ( $R_{\text{arc}}$ ). Since arc core radius is not constant along the axial direction, the mentioned arc core radius corresponds to the arc core radius very near to the cathode/inlet in type II geometry. Radius of the cathode tip in type II geometry is 0.5 mm and it is kept constant for all cases. In type I geometry, arc core radius ( $R_{\text{arc}}$ ) and arc length ( $L_{\text{arc}}$ ) are assumed, respectively, as the radial distance along the cathode from the centerline to the point at which current density is zero and as the axial distance from the cathode at which current density is zero to the distance at which the center of the anode-arc spot at the wall is located (Fig. 2). The arc core radius ( $R_{\text{arc}}$ ) and arc length ( $L_{\text{arc}}$ ) in type II geometry are assumed, respectively, as the radial distance along cathode tip and inlet from the centerline to the point at which current density is zero and as an axial distance from the cathode tip/inlet to the distance at which the center of the anode-arc spot at the wall is located.

In type I geometry, the temperature at the cathode is 3500 K if  $r \leq R_{\text{arc}}$  otherwise radial profile of the temperature along the cathode is given by

$$T(r) = 3200 \times \left[ 1 - \left( \frac{r - R_{\text{arc}}}{R_{\text{max}} - R_{\text{arc}}} \right)^n \right] + 300, \quad (\text{Eq 5})$$

where  $R_{\text{max}}$  and  $n$  are  $4.0 \times 10^{-3} \text{ m}$  and 2.0, respectively. The temperature of the cathode tip is assumed as 3500 K in type II geometry. The temperature of the plasma gas entering at the inlet are assumed in type I and type II

**Table 2** Boundary conditions used in type I and type II geometries

Boundary	Temperature	Velocity $V_i$	Electric potential, $\phi$	Magnetic potential, $A_i$
Inlet	300 K (type I) 3500 K (type II)	Mass flow rate, kg/s	$\partial\phi/\partial n = 0$ (type I) $j(r)$ (type II)	$\partial A_i/\partial n = 0$
Cathode/ Cathode tip	3500 K up to $r = R_{\text{arc}}$ & $T(r)$ (type I) 3500 K (type II)	0.0	$j(r)$	$\partial A_i/\partial n = 0$
Anode	$Q_a = h_{\text{conv}}(T_{\text{wall}} - T_{\text{water}})$	0.0	$(\phi = 0 \text{ at spot})$ $\partial\phi/\partial n = 0$	$\partial A_i/\partial n = 0$
Outlet	$\partial T/\partial n = 0$	$\partial V_i/\partial n = 0$	$\partial\phi/\partial n = 0$	0.0

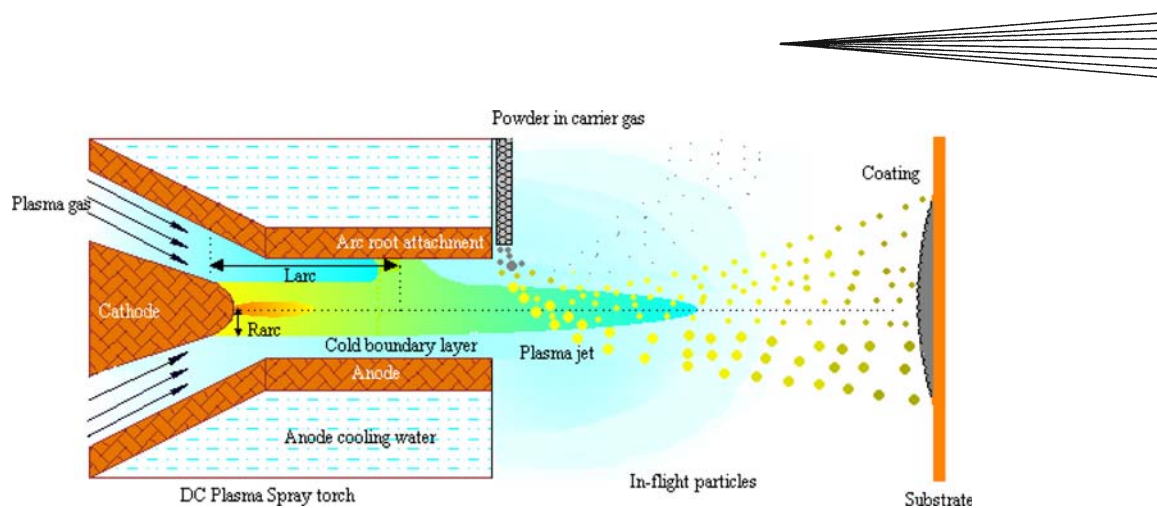


**Fig. 2** Schematic view of a steady state arc inside the DC nontransferred torch

geometries as 300 and 3500 K (Ref 17), respectively. Other boundary conditions are the same in both geometries. Since temperature very near to the wall is low, temperature dependent electrical conductivity is also lowered, which limits the flow of electric current through the electrodes. In order to avoid this problem, harmonic mean electrical conductivity between plasma and anode material is assumed at the cells adjacent to the anode wall (Ref 12, 15). At the anode spot and wall, electric potential and gradient of electric potential are assumed to zero, respectively. These boundary conditions make an arc current pass through anode spot only. Heat flux to the anode wall due to electron condensation, electron enthalpy transport, and conductive heat transfer is given by (Ref 12, 17, 26, 27)

$$Q_a = j\phi_w + \frac{5k_B}{2e}jT - \lambda \left. \frac{\partial T}{\partial r} \right|_{\text{wall}} = h_{\text{conv}}(T_{\text{wall}} - T_{\text{water}}), \quad (\text{Eq 6})$$

Here  $\phi_w$ ,  $k_B$ , and  $e$  are the work function of the anode material, Boltzmann's constant, and the electron charge, respectively. Heat flux to the anode wall due to ion recombination is neglected since its contribution is about 5% of the total heat flux to the anode (Ref 26, 27). But heat flux to the anode by the radiation cannot be neglected. Since plasma is considered as optically thin, it is assumed that the total energy lost by the plasma through radiation is taken by the anode wall. Hence, heat flux to the anode due to the radiation is included in the left hand side of Eq 6. The radiation from the wall is also negligible since entire wall has a quite low temperature except arc spot. The convective heat transfer coefficient of cooling water  $h_{\text{conv}}$  is assumed as  $2.0 \times 10^5 \text{ W/m}^2 \text{ K}$  (Ref 12, 13, 17).  $T_{\text{wall}}$  and  $T_{\text{water}}$  are, respectively, the local temperature of the wall and the temperature of the cooling water (300 K).

In the nontransferred arc, both arc length and arc core radius adjust themselves for the torch power that corresponds to given gas flow and arc current. For the same arc core radius, arc length is varied until the measured torch power, which corresponds to the given gas flow rate and current, is obtained. Similarly different arc lengths that can generate the same torch power are determined for

**Table 3** Dependent variable/property ( $\phi$ ), diffusion coefficient ( $\Gamma_\phi$ ), and source term ( $S_\phi$ ) in each equation used to simulate the plasma jet

Equation	$\phi$	$\Gamma_\phi$	$S_\phi$
Continuity	1	0	0
Momentum	$u, v, \& w$	$\mu_t + \mu_t$	$-\nabla P$
Energy	$h$	$\lambda/Cp + \mu_t/Pr_{t,h}$	$-S_R$
Mass fraction	$y$	$\lambda/Cp + \mu_t/Pr_t$	0
Kinetic energy	$K$	$\mu_t + \mu_t/Pr_{t,K}$	$\rho(P_K - \varepsilon)$
Dissipation rate	$\varepsilon$	$\mu_t + \mu_t/Pr_{t,\varepsilon}$	$\rho(\varepsilon/K)(C_1P_k - C_2\varepsilon)$

different arc core radii in the same gas flow rate and current. At last, a combination of arc core radius and arc length, which corresponds to the real size of the arc, is determined using the original principle of minimum entropy production (Ref 28, 29). This principle states that a system, kept by an external agent in stationary nonequilibrium state not far from thermo-dynamical equilibrium, adjusts itself to a state in which the entropy production is a minimal. The proof of this theorem is given in Ref 17. The derived equation Eq 7 used to calculate entropy production ( $\Sigma$ ) in an arc channel is (Ref 17)

$$\Sigma = \int_{A_{\text{wall}}} \frac{1}{T} \vec{J}_{\text{th}} \cdot d\vec{A} + \int_{A_{\text{cross}}} \frac{1}{T} \vec{J}_{\text{th}} \cdot d\vec{A} + \int_{A_{\text{cross}}} \frac{1}{T} \rho h \vec{V} \cdot d\vec{A} + \int_V \frac{\rho h}{T^2} (\vec{V} \cdot \nabla T) dv \quad (\text{Eq 7})$$

## 2.2 Plasma Jet

Plasma jet is simulated by assuming plasma jet is steady, in local thermodynamical equilibrium, optically thin, incompressible, turbulent, and mass diffusivity is equal to thermal diffusivity. Ar-N<sub>2</sub> plasma jet is discharged into air at an atmospheric condition. Table 3 shows an appropriate  $\phi$ ,  $\Gamma_\phi$ , and  $S_\phi$  for continuity, momentum, energy and species equations that can be derived from Eq 1. In Table 3,  $K$ ,  $\varepsilon$ ,  $y$ ,  $Pr$ ,  $P_K$ ,  $\mu_t$ ,  $C_1$ , and  $C_2$  are turbulent kinetic energy, its dissipation rate, mass fraction, Prandtl number, production rate of turbulent

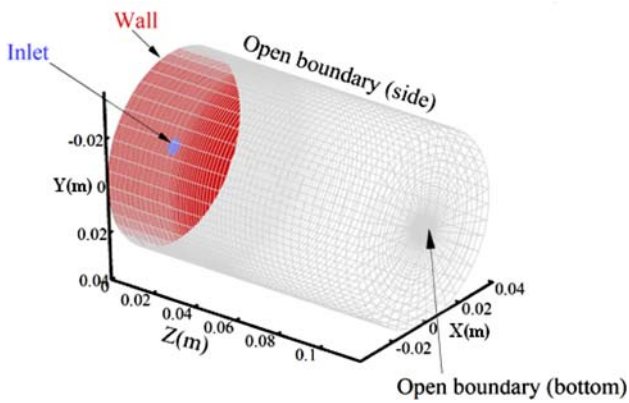


Fig. 3 Computational geometry to simulate plasma jet

Table 4 Details of the experiments

Case	Current, A	Voltage, V	Ar, slpm	N <sub>2</sub> , slpm	Power, kW	Efficiency, %
A	400	40	25	3	16	47.93
B	500	42.7	20	3	21.35	48.78
C	500	40.2	25	3	20.10	48.19
D	500	34	30	3	17	47.16
E	600	37	25	3	22.20	46.64

kinetic energy, turbulent viscosity, 1.44 (model constant), and 1.92 (model constant), respectively. Standard  $K-\epsilon$  model (Ref 30) is used to account the turbulent characteristics of the plasma jet.

Figure 3 shows the computational domain used to simulate the plasma jet. It is discretized in to 1,56,240 calculation points. Mesh is refined at core region of the jet. The nozzle exit diameter is 7.0 mm at the top boundary and the remaining top boundary is anode wall that is fixed to 500 K. The temperature and velocity profiles at the nozzle exit are taken from the simulation results of plasma arc model. The  $K$  and  $\epsilon$  at the inlet are given as 0.005 times of square of the velocity and 0.1 times of square of  $K$ , respectively (Ref 30). If the flow is entering into the computational domain at open boundaries, atmospheric air is assumed to enter. If the flow is leaving computational domain at these boundaries, gradient of all variables is zero other than pressure. Governing equations are solved by SIMPLE algorithm used in commercial CFD software FLUENT 6.3.

### 3. Results and Discussion

#### 3.1 Plasma Arc

Experiments were carried out in 40 kW plasma spray torch. A mixture of argon and nitrogen with different compositions was used as a plasma gas. For given current and gas flow rate of argon and nitrogen, the measured arc voltage and electro-thermal efficiency of the torch are

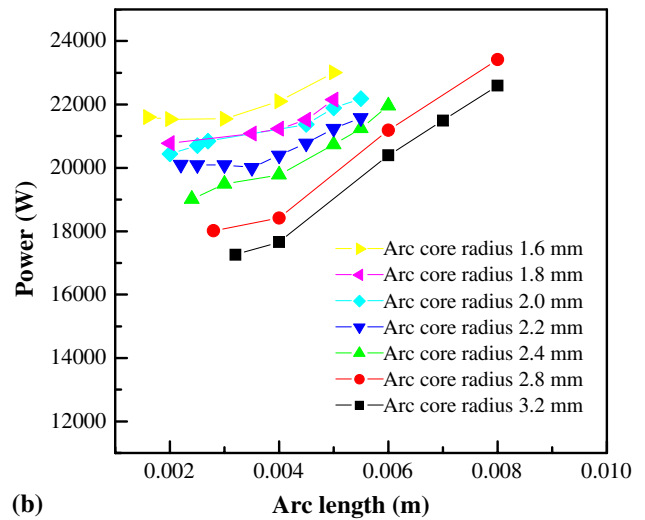
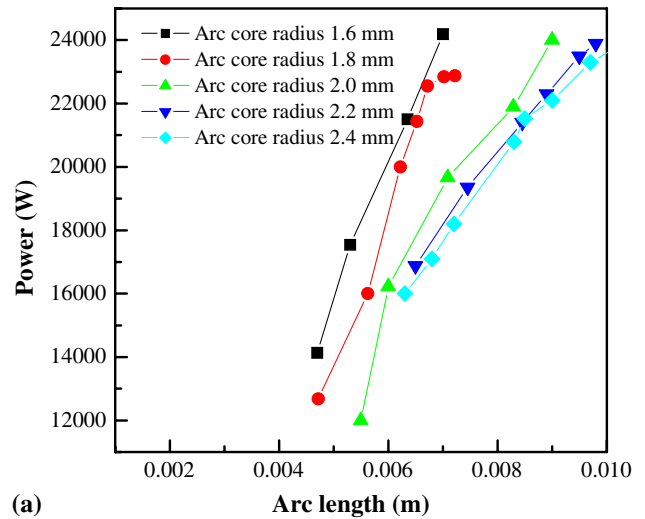
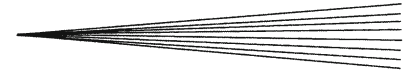


Fig. 4 Effect of arc length on torch power for various arc core radii in (a) type I and (b) type II geometries (case B)

shown in Table 4. The arc current and voltage across the torch electrodes and water temperatures at the torch inlet and outlet were measured as a function of time using PC-based data acquisition system (Data Acquisition Card PCI-1202H—ICP-DAS, Taiwan). Resistance temperature detectors (RTD) were used to measure the temperature. The same input parameters are used for simulations and measured voltages and electro-thermal efficiencies of the torch are used to validate the present model. Although there are small fluctuations in voltage, the cases mentioned in Table 4 are almost steady. The measured voltage and electro-thermal efficiency are time averaged one and the same are used for simulations. Moreover, principle of minimum entropy production cannot be used for unsteady flow. Hence steady state is assumed in the present model.

The effect of arc length on torch power in type I and type II geometries is shown in Fig. 4(a) and (b), respectively, for various arc core radii. The current and gas flow



rate used here are 500 A and 20 slpm of argon and 3 slpm of nitrogen (case B). Results obtained in both geometries show that torch power increases with increasing the arc length irrespective of arc core radius, whereas the same decreases with increasing the arc core radius. However, the effect of arc length on power is stronger in type I geometry (Fig. 4a) than that in type II geometry (Fig. 4b). This may be due to different definition of arc core radius and arc length used in type I and type II geometries. It is noticed that different combinations of arc length and arc core radius can match the same torch power in both geometries. For example, measured torch power of 21.35 kW (case B) is obtained from five different combinations of arc core radius and arc length in type I geometry and seven different combinations of arc core radius and arc length in type II geometry. It is difficult to match power if the arc core radius is greater than 2.4 mm in type I geometry. In the same way, various combinations of arc length and arc core radius to obtain the power given to the torch are predicted at various current and gas flow rates (cases A-E). From the possible combinations of the arc core radius and arc length predicted for given current and gas flow rate, the most feasible combination of the same is obtained by using original principle of minimum entropy production.

The combinations of arc core radius and arc length that generate the torch power corresponds to given current and gas flow rate and entropy production for each combination of the same are shown in Fig. 5. Results of the type I geometry show that arc length increases or decreases with increasing arc core radius to generate the torch power that corresponds to given current and gas flow rate. In type II geometry, arc length increases with increase in arc core radius whereas the same effect is not seen at shorter and longer arc core radii in type I geometry. The variation of arc length with arc core radius in type I geometry is not similar to that in type II geometry for complete range of arc core radius. This is because different definitions used for arc length and arc core radius and boundary conditions used at cathode and inlet in these geometries. Entropy production increases with increasing the current (compare case A, case C, and case E) whereas the same decreases with increasing the gas flow rate (compare case B, case C, and case D) in both geometries. Minimum entropy production is obtained at particular combination of arc core radius and arc length in type I geometry whereas the same is obtained only for case B in type II geometry. Because of higher gas flow rate and lower power in case D, any arc lengths for an arc core radius from 1.6 to 3.2 mm, produce the power more than 17 kW. Further if the arc length is less than the arc core radius, convergence problem is occurred. Hence, in type II geometry, measured torch power could be obtained with only one combination of arc length and arc core radius for case D.

Arc length increases with increasing current and decreasing gas flow rate where at minimum entropy production in type I geometry. These results oppose the experimental (Ref 2) and previous numerical (Ref 9, 20) results. These results are qualitatively explained through

a current conservation equation Eq 8, derived by Ramachandran et al. (Ref 17), as follows:

$$L_{\text{arc}} = \pi R_{\text{arc}}^2 \sigma \frac{W}{I^2} \quad (\text{Eq 8})$$

If the current ( $I$ ) is increased, ratio of torch power ( $W$ ) to square of the arc current ( $W/I^2$ ) decreases the arc length by a factor  $10^{-2}$ . Since minimum entropy production is obtained at the same arc core radius for all currents, arc core radius does not have any influence here (by assuming radial diffusion of arc core is negligible). When the current is increased from 400 to 600 A, an average temperature of an arc is increased from 11500 to 14000 K. Since the effect of temperature on the electrical conductivity is very strong in this region, the change in electrical conductivity for a change in 1000 K is over 20%. Hence arc length increases with increasing current. If the gas flow rate is increased, torch power, an average temperature, and corresponding electrical conductivity of the plasma are decreased. Since there is a strong change in electrical conductivity for a small change in the power, arc length is decreased while increasing the gas flow rate though arc core radius has little opposite effect. Although the present results could be explained from a current conservation equation, it is believed that the same are due to the direct consequence of assuming validity of the principle of minimum entropy production used in this model.

The effect of current and gas flow rate on arc length cannot be explained from the results of type II geometry since minimum entropy production is obtained for case B only. Though type II geometry is simpler than type I geometry to simulate the arc, an inability to obtain different combinations of arc core radius and arc length for case D and the same to obtain minimum entropy production for cases other than B are considered as drawbacks of type II geometry.

Figure 6 shows the temperature and velocity distributions inside the torch predicted in type I and type II geometries for case B. Since minimum entropy production is observed only for case B in type II geometry, it is taken for comparison. Since the arc attaches at particular spot in an anode, three-dimensional effect is clearly seen in both temperature and velocity fields. Predicted temperature near the spot is higher in type I geometry than the same in type II geometry. This is because convective force near the anode wall is greater in type II geometry than that in type I geometry. Predicted velocity is higher in type II geometry than that in type I geometry. Velocities show larger difference than temperatures. Nozzle exit temperature and velocity profiles obtained from type I and type II geometries are shown in Fig. 7(a) and (b), respectively. Three-dimensional effect is stronger in both profiles obtained from type I geometry than that obtained from type II geometry. Velocity shows stronger three-dimensional effect and more pronounced peak at the center than temperature.

Torch efficiencies predicted at minimum entropy production in type I and type II geometries are shown in Table 5 for different cases. In type II geometry, predicted efficiency at minimum entropy production is given for

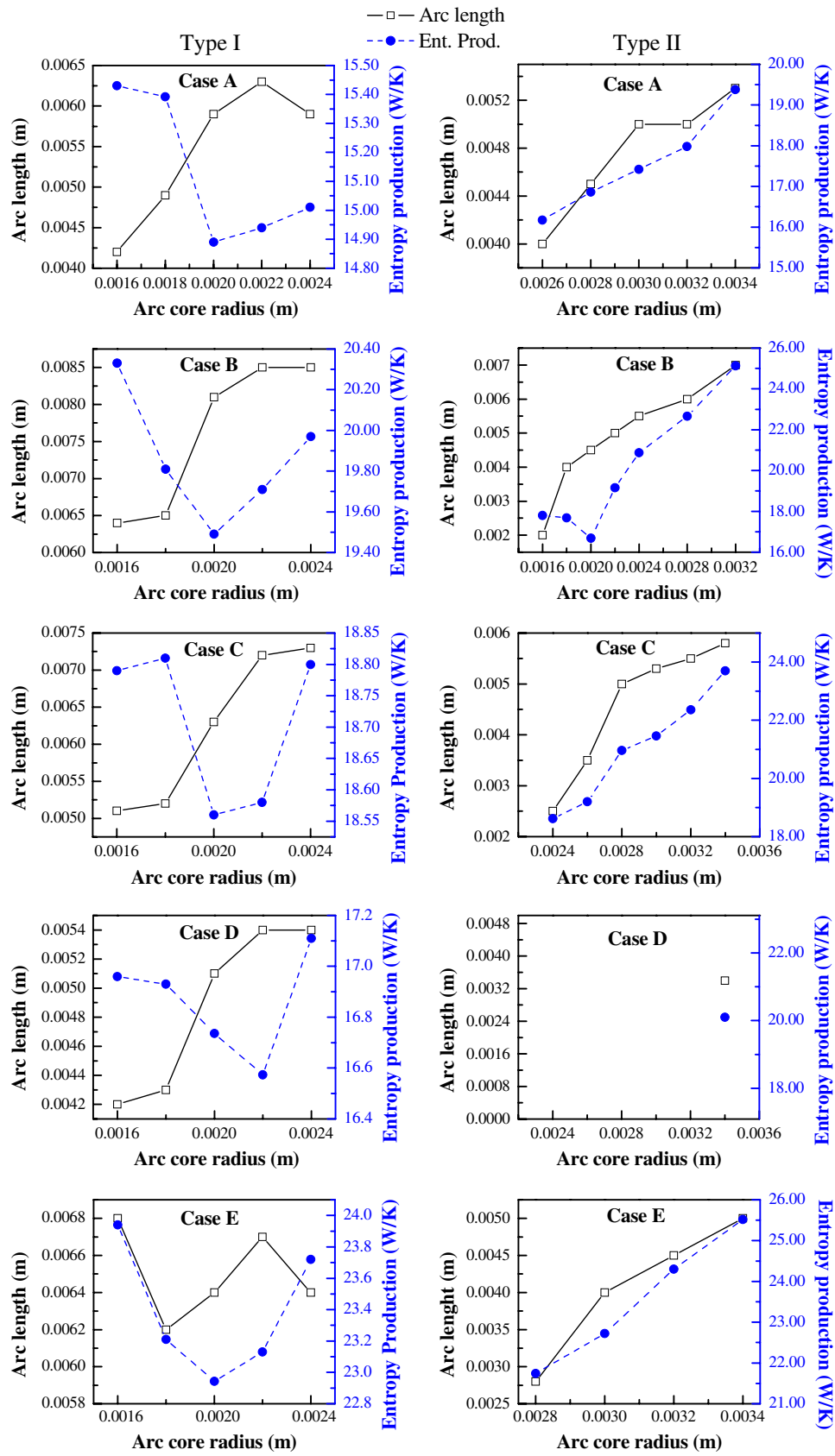


Fig. 5 Combinations of arc core radius and arc length and its effect on entropy production

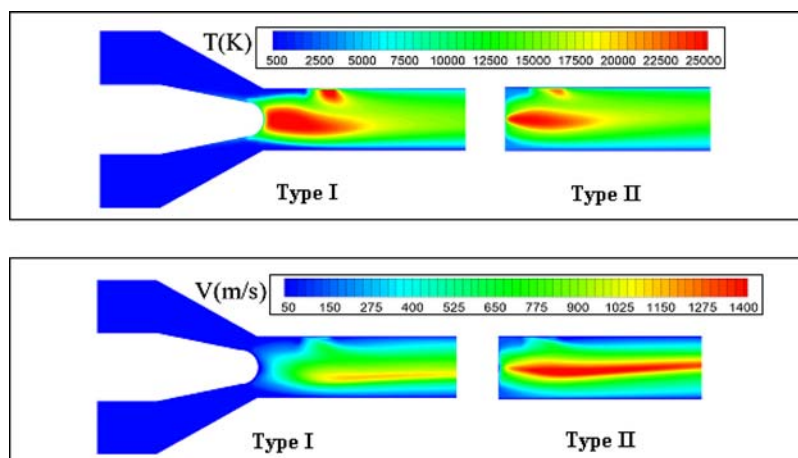


Fig. 6 Predicted temperature and velocity distributions in type I and type II geometries at minimum entropy production

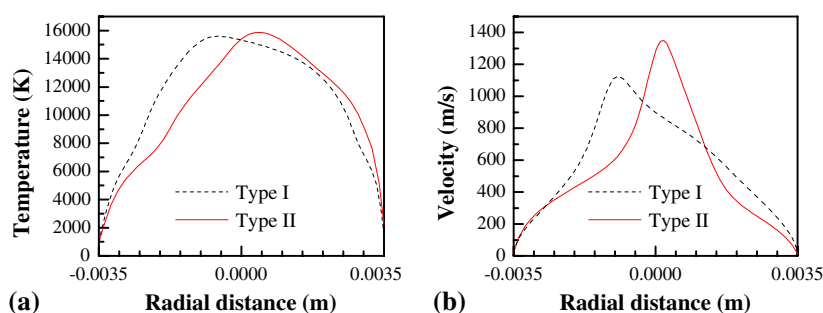


Fig. 7 Nozzle exit (a) temperature and (b) velocity profiles (at  $X=0$  plane) obtained from type I and type II geometries

Table 5 Comparison of predicted and measured efficiencies

Case	Measured efficiency, %	Predicted efficiency, %	
		Type I	Type II
A	47.9	44.6	53.4
B	48.8	46.3	49.9
C	48.2	45.5	51.7
D	47.2	39.9	50
E	46.6	41.6	49.7

case B and for other cases, average efficiency at same torch power with different combinations of arc core radius and arc length is given. Torch efficiencies are under predicted in type I geometry whereas the same are over predicted in type II geometry. However efficiencies predicted in both geometries are comparable with measured efficiencies. The difference between efficiencies predicted in type I and type II geometries is due to the difference between cathode losses. Cathode loss in type I geometry is around 10% whereas the same is around 1% in type II geometry.

Figure 8 shows the potential distribution predicted in type I and type II geometries for case B. Comparison between measured and predicted arc voltages is given in

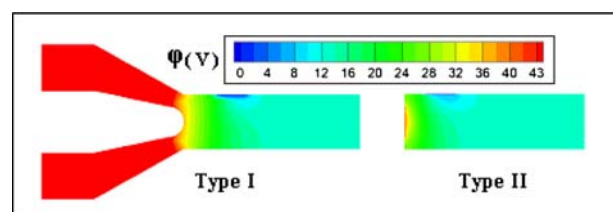


Fig. 8 Predicted potential distribution in type I and type II geometries for case B

Table 6. Since minimum entropy production is obtained only for case B in type II geometry, average values of potential difference (voltage) are given for other cases. Potential differences predicted in both geometries are in good agreement with the experimental results. Also, in order to show the validity of the present model, present results are compared with previous numerical results (Ref 12). Figure 9(a) and (b) shows the temperature and velocity of the argon plasma at the nozzle exit, respectively, for the current of 400 A and gas flow rate of 2.0 STP  $\text{m}^3/\text{h}$ . The present results are comparable with previous results. Moreover, maximum temperature and velocity predicted by the present model are closer to the centerline than that predicted by the previous model.

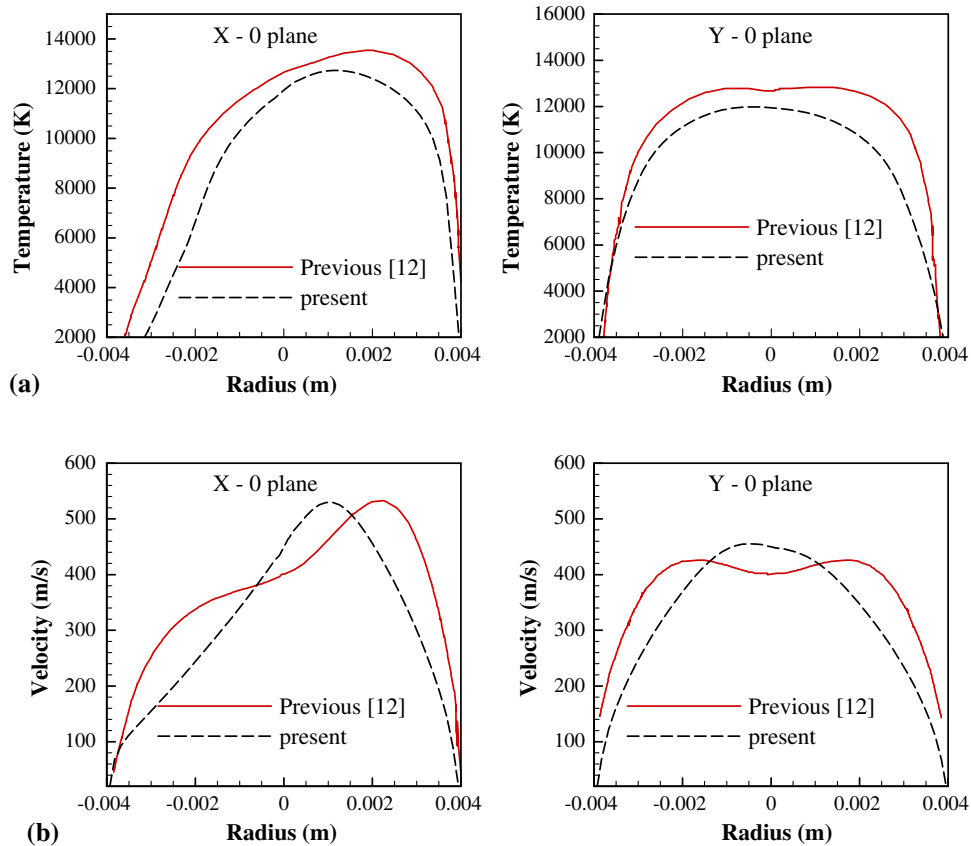
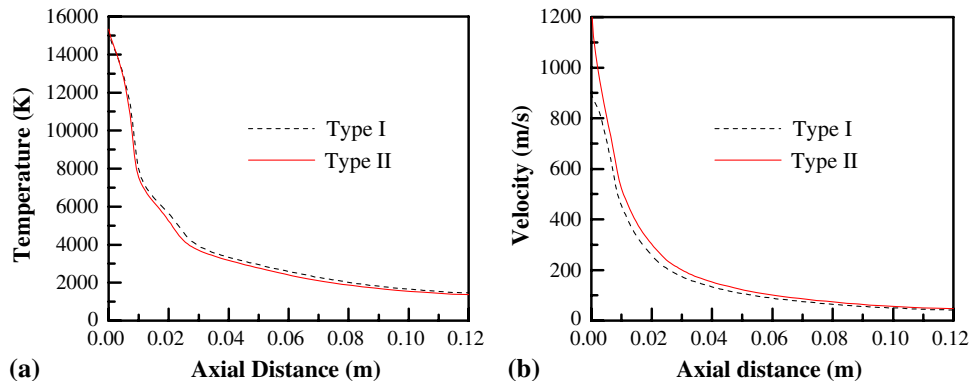


**Table 6** Comparison of predicted and measured arc voltages

Case	Measured voltage, V	Predicted voltage, V	
		Type I	Type II
Case A	40	41	41.3
Case B	42.7	42.9	43
Case C	40.2	41.4	41.6
Case D	34	34.4	34.8
Case E	37	38	38.2

### 3.2 Plasma Jet

Figure 10(a) and (b) shows the plasma jet temperature and velocity along the axial direction. The nozzle exit temperature and velocity profiles are taken from type I and type II geometries to simulate the plasma jet. Both temperatures and velocities of the plasma jet simulated from the nozzle exit temperature and velocity profiles predicted from both type I and type II geometries show similar variation along the axial direction. Difference between centerline temperatures of the plasma jet is lower

**Fig. 9** Nozzle exit (a) temperature and (b) velocity profiles of the argon plasma**Fig. 10** Centerline (a) temperature and (b) velocity of the plasma jet simulated from the nozzle exit profiles of type I and type II geometries

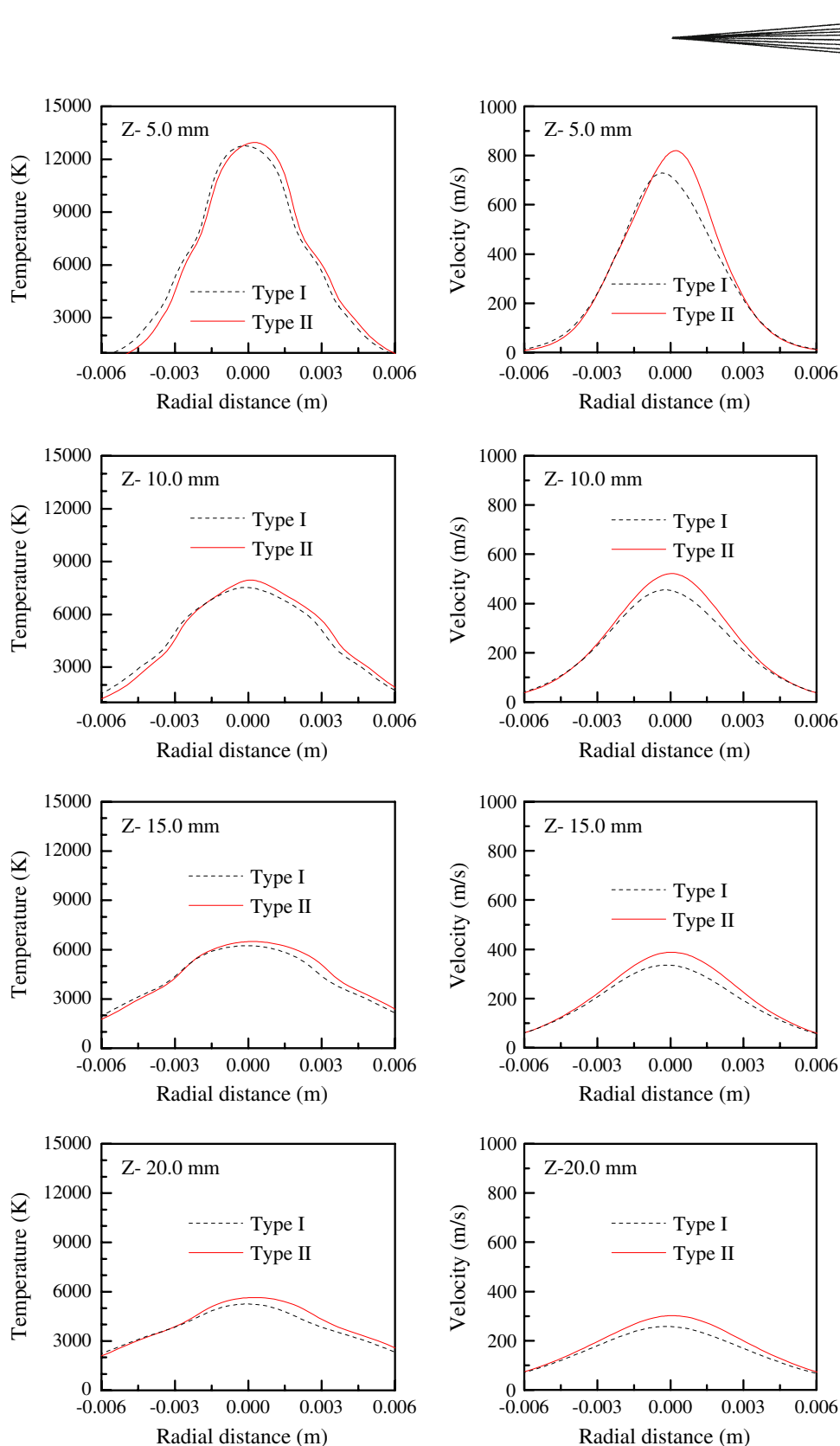


**Fig. 11** Radial distribution of temperature and velocity of the plasma jet at different axial distances ( $Z$ )

than that between centerline velocities. This is because the higher velocity is predicted at the nozzle exit in type II geometry. The difference between velocities of the plasma

jet simulated from the nozzle exit profiles of type I and type II geometries decreases with increasing axial distance.

Radial distribution of plasma jet temperature and velocity at different axial distances is shown in Fig. 11. Though three-dimensional effect is stronger in both velocity and temperature near the nozzle exit, it decays along the axial direction. It is noticed that there is a small difference between temperatures and velocities of the plasma jet simulated from the nozzle exit profiles of type I and type II geometries even in the downstream. Due to turbulent mixing of Ar-N<sub>2</sub> plasma with cold air, the difference between velocities observed at the nozzle exit decrease along the axial direction. From these results, it is concluded that if the particles are injected into the plasma jet simulated from the nozzle exit profiles of type I and type II geometries, almost the same temperature and different velocities of the particles may be predicted.

#### 4. Conclusion

A three-dimensional plasma arc model is developed to simulate the arc in two different geometries of the non-transferred plasma torch. Plasma arc characteristics predicted in type I and type II geometries are compared. Also, temperature and velocity distributions of the plasma jets simulated from the nozzle exit profiles of these geometries are compared. The following conclusions are arrived from this study.

1. Arc length and arc core radius are adjusted to obtain the torch power that corresponds to given current and gas flow rate. Various combinations of arc length and arc core radius match the same torch power.
2. Different combinations of arc length and arc core radius for case D and the minimum entropy production for the cases other than B could not be predicted in type II geometry.
3. Predicted temperature near the anode spot in type I geometry is higher than that in type II geometry. Predicted velocity is higher in type II geometry than that in type I geometry.
4. Velocity shows stronger three-dimensional effect and more pronounced peak at the nozzle exit than temperature.
5. Particles injected into the plasma jets simulated from the nozzle exit profiles of type I and type II geometries may get almost the same temperature and different velocities.
6. Predicted torch efficiencies and arc voltages in type I and type II geometries are comparable with measured one.

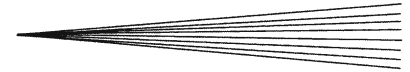
#### Acknowledgments

The research grand provided by BRNS, Department of Atomic Energy, Mumbai, India for this study is acknowledged. The authors wish to thank Dr. P.V. Ananthapadmanabhan, Bhabha Atomic Research Centre,

Mumbai, India for his help to carryout the experiments in his laboratory.

#### References

1. Z. Duan and J. Heberlein, Arc Instabilities in a Plasma Spray Torch, *J. Therm. Spray Technol.*, 2002, **11**, p 44-51
2. S.A. Wutzke, E. Pfender, and E.R.G. Eckert, Symptomatic Behaviour of an Electric Arc with a Superimposed Flow, *AIAA J.*, 1968, **6**, p 1474-1482
3. J.L. Dorier, C. Hollenstein, A. Salito, M. Loch, and G. Barbezat, Characterisation and Origin of Arc Fluctuations in a F4 dc Plasma Torch Used for Thermal Spraying, *High Temp. Mater. Process.*, 2001, **5**, p 477-489
4. J.L. Dorier, M. Gindrat, C. Hollenstein, A. Salito, M. Loch, and G. Barbezat, Time-Resolved Imaging of Anodic Arc Root Behavior During Fluctuations of a DC Plasma Spraying Torch, *IEEE Trans. Plasma Sci.*, 2001, **29**, p 494-501
5. E. Nogues, M. Vardelle, P. Fauchais, and P. Granger, Arc Voltage Fluctuations: Comparison Between Two Plasma Torch Types, *Surf. Coat. Technol.*, 2008, **202**, p 4387-4393
6. X. Tu, J.H. Yan, B.G. Cheron, and K.F. Chen, Fluctuations of DC Atmospheric Double Arc Argon Plasma Jet, *Vacuum*, 2008, **82**, p 468-475
7. H. Huang, W. Pan, and C. Wu, Arc Root Motion in an Argon-Hydrogen DC Plasma Torch, *IEEE Trans. Plasma Sci.*, 2008, **36**, p 1050-1051
8. R. Westhoff and J. Szekeley, A Model of Fluid, Heat Flow, and Electromagnetic Phenomena in a Nontransferred Arc Plasma Torch, *J. Appl. Phys.*, 1991, **70**, p 3455-3466
9. S. Paik, P.C. Huang, J. Heberlein, and E. Pfender, Determination of the Arc-Root Position in a DC Plasma Torch, *Plasma Chem. Plasma Process.*, 1993, **13**, p 379-397
10. A.B. Murphy and P. Kovitya, Mathematical Model and Laser-Scattering Temperature Measurements of a Direct-Current Plasma Torch Discharging into Air, *J. Appl. Phys.*, 1993, **73**, p 4759-4769
11. J.J. Gonzalez, P. Freton, and A. Gleizes, Comparisons Between Two- and Three-Dimensional Models: Gas Injection and Arc Attachment, *J. Phys. D Appl. Phys.*, 2002, **35**, p 3181-3191
12. H.P. Li, E. Pfender, and Xi. Chen, Application of Steenbeck's Minimum Principle for Three-Dimensional Modelling of DC Arc Plasma Torches, *J. Phys. D Appl. Phys.*, 2003, **36**, p 1084-1096
13. C. Baudry, A. Vardelle, and G. Mariaux, Numerical Modeling of a dc Non-transferred Plasma Torch: Movement of the Arc Anode Attachment and Resulting Anode Erosion, *High Temp. Mater. Process.*, 2005, **9**, p 1-15
14. E. Moreau, C. Chazelas, G. Mariaux, and A. Vardelle, Modeling the Restrike Mode Operation of a DC Plasma Spray Torch, *J. Therm. Spray Technol.*, 2006, **15**, p 524-530
15. J.P. Trelles and J.V.R. Heberlein, Simulation Results of Arc Behavior in Different Plasma Spray Torches, *J. Therm. Spray Technol.*, 2006, **15**, p 563-569
16. C. Chazelas, E. Moreau, G. Mariaux, and A. Vardelle, Numerical Modeling of Arc Behavior in a dc Plasma Torch, *High Temp. Mater. Process.*, 2006, **10**, p 393-406
17. K. Ramachandran, J.L. Marquès, R. Vaßen, and D. Stöver, Modelling of Arc Behaviour Inside a F4 APS Torch, *J. Phys. D Appl. Phys.*, 2006, **39**, p 3323-3331
18. J.P. Trelles, E. Pfender, and J.V.R. Heberlein, Modelling of the Arc Reattachment Process in Plasma Torches, *J. Phys. D Appl. Phys.*, 2007, **40**, p 5635-5648
19. J. Park, J. Heberlein, E. Pfender, C. Candler, and C.H. Chang, Two-Dimensional Numerical Modeling of Direct-Current Electric Arcs in Nonequilibrium, *Plasma Chem. Plasma Process.*, 2008, **28**, p 213-231
20. H.P. Li and E. Pfender, Three Dimensional Modeling of the Plasma Spray Process, *J. Therm. Spray Technol.*, 2007, **16**, p 245-260
21. I.B. Matveev, A.A. Tropina, S.I. Serbin, and V.Y. Kostyuk, Arc Modeling in a Plasmatron Channel, *IEEE Trans. Plasma Sci.*, 2008, **36**, p 293-298



22. J.F. Coudert and V. Rat, Influence of Configuration and Operating Conditions on the Electric Arc Instabilities of a Plasma Spray Torch: Role of Acoustic Resonance, *J. Phys. D Appl. Phys.*, 2008, **20**, p 10
23. D.L. Evans and R.S. Tankin, Measurement of Emission and Absorption of Radiation by an Argon Plasma, *Phys. Fluid*, 1967, **10**, p 1137-1144
24. V.R. Waston and E.B. Pegot, Numerical Calculations for the Characteristics of a Gas Flowing Axially Through a Constricted Arc. NASA Tech. Note D-4042, 1967
25. A.B. Murphy and C.J. Arundell, Transport Coefficients of Argon, Nitrogen, Oxygen, Argon-Nitrogen, and Argon-Oxygen Plasmas, *Plasma Chem. Plasma Process.*, 1994, **14**, p 451-490
26. T. Amakawa, J. Jenista, J. Heberlein, and E. Pfender, Anode-Boundary-Layer Behaviour in a Transferred, High-Intensity Arc, *J. Phys. D: Appl. Phys.*, 1998, **31**, p 2826-2834
27. J. Jenista, J.V.R. Heberlein, and E. Pfender, Numerical Model of the Anode Region of High-Current Electric Arcs, *IEEE Trans. Plasma Sci.*, 1997, **25**, p 883-890
28. Th. Peters, On the Relationship Between Steenbeck Minimum Principle and the Thermo Dynamical Principle of Minimum Entropy Production, *Z. Phys.*, 1956, **144**, p 612-631
29. S.R. de Groot and P. Masur, *Non-Equilibrium Thermodynamic*, Dover Publications, New York, NY, 1984
30. H.P. Li and X. Chen, Three-Dimensional Simulation of a Plasma Jet with Transverse Particle and Carrier Gas Injection, *Thin Solid Films*, 2001, **390**, p 175-180